Thermally Controlled Electrochemical CMOS Microsystem for Protein Array Biosensors

Xiaowen Liu, *Student Member, IEEE*, Lin Li, and Andrew J. Mason, *Senior Member, IEEE*

***Abstract*—Because many proteins useful in biosensors exhibit temperature dependent activity, this paper explores the opportunity to integrate thermal control within a protein array biosensor microsystem. A CMOS microhotplate array tailored to protein interfaces was developed for thermoregulation in a liquid sample environment. The microhotplates were shown to provide suitable thermal control for biosensor temperature ranges without the process complexity of most previously reported microhotplates. When combined with a CMOS analog thermal controller, the on-chip array was shown to set and hold temperatures for each protein site within $\pm 1^\circ$ C, and array elements were found to be almost completely thermally isolated from each other at distances beyond 0.4 mm. The compact size and low power of this controller enable it to be combined with the thermal control structures and instantiated for every element in a sensor array to increase biosensor interrogation throughput.**

***Index Terms*—Biosensor, microhotplate, microsystem, protein array, thermal control.**

I. Introduction

PROTEINS are vital entities in human cells and are involved in nearly all body functions both in healthy and diseased individuals [1]. For example, proteins are used to control senses, move muscles, digest food, and fight against infections and process emotions. The study of the role that proteins play in biological operations is referred to as proteomics. Characterization of protein structure and function is critical to the field of proteomics and leads to important developments in many bio/medical applications including drug discovery, biosensor technologies, and clinical and forensic analysis. Recently, protein characterization using high-throughput protein array methods have been explored as the next-generation evolution of DNA microarrays by allowing rapid, direct and quantitative measurement of a wide range of biomolecules [2], [3]. Protein array technology takes advantage of the fact that a large number of targets can be analyzed in parallel measurements with low sample consumption, which is especially important because biological samples preparation can be very costly. Furthermore, protein arrays enable comparative analyses of several different samples within a single array chip. For example, in medical research, many diagnostic parameters of interest can be analyzed in parallel, saving significant time and money.

Miniaturized, electrochemical biosensors have shown great promise for minimizing the size and power of protein arrays, enabling their use in vital applications such as point-of-care diagnostics. However, as size scales down to form high density arrays, the response signal of electrochemical biosensors become very weak ($\sim$fA $-$ pA). Integrating biosensor elements directly with electrochemical instrumentation electronics is an effective method to provide miniaturization while minimizing the effects of external noise and ultimately maximizing signal resolution [4]. Such a miniaturized analysis tool would improve efficiency and speed of analysis, reduce reagent usage, allow portability, and improve sensing limits of detection [5], [6].

Protein activity is highly temperature dependent, typically doubling every 10°C (within the biological temperature window) [7]. Thus, temperature dependence is a very important parameter to study during protein characterization. Furthermore, thermal control can be utilized to maximize the sensitivity of protein-based sensors. Numerous "microhotplates", miniaturized heating and temperature sensing structures, have been demonstrated, particularly for gas sensors, using CMOS technology [8]–[10]. However, no thermal control structures suitable for miniaturized protein arrays operated in a liquid environment have been reported.

This paper presents the first known all-CMOS programmable thermal control microsystem that permits electrochemical readout and the simultaneous setting of individual protein array sites to different temperatures across a range suitable for biological interfaces, without post-CMOS processing. This microsystem was developed through two design generations: an initial CMOS microhotplate array [11] and a second generation chip that adds CMOS electronics for on-chip temperature controller and electrochemical readout and a packaging scheme for operation within liquid environments. Because the optimal activities of different classes of protein occur at different environmental temperatures [12]–[17], the unique ability to heat individual sites and measure multiple proteins at different temperatures in parallel is a valuable capability that can significantly reduce the experiment time and cost [18]. Furthermore, the unique abilities of this chip are useful for other applications, including determination of DNA melting temperature for analysis of ligand binding or other factors enhancing/disturbing DNA thermal stability [19], [20] and detection of thermal state transitions of DNA hairpins [21].

Manuscript received April 30, 2013; revised July 23, 2013; accepted October 23, 2013. Date of publication February 24, 2014; date of current version March 25, 2014. This project was supported by the National Science Foundation under award DBI-0649847 and the NSF Engineering Research Centers Program under award EEC-9986866. This paper was recommended by Associate Editor J. Chen.

The authors are with the Department of Electrical and Computer Engineering, Michigan State University, East Lansing, MI 48824 USA (e-mail: mason@msu.edu).

Color versions of one or more of the figures in this paper are available online at http://ieeexplore.ieee.org.

Digital Object Identifier 10.1109/TBCAS.2013.2291226

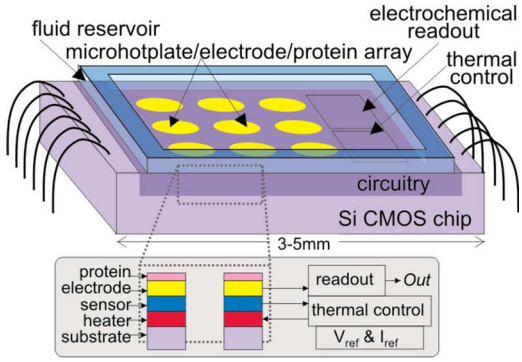

Fig. 1. Conceptual view of the thermally controlled protein biosensor array on a CMOS microsystem platform. The bottom inset shows the layers within each array element and connections to CMOS circuitry.

The architecture of the CMOS thermally controlled electrochemical microsystem is introduced in Section II. The design of a CMOS microhotplate array that provides the heating capabilities, thermal uniformity, and thermal isolation desired for protein interfaces is presented in Section III. CMOS circuitry for autonomous thermal control of the hotplate array and electrochemical readout of protein interfaces is discussed in Section IV. Section V describes the post-CMOS fabrication of a chip-in-package encapsulation system that enables operation in a liquid environment necessary for biological interfaces. Finally, test results are presented in Section VI.

II. System Architecture

In recent years, miniaturized lab-on-chip and micro total analysis systems have been introduced for biochemical analyses in drug screening and the development of novel therapies using a variety of micro- and nano- technologies [22], [23]. The fluid handling capabilities of these miniaturized biosensor arrays provide significant advantages in terms of cost and throughput. However, to fully realize the potential of these devices, a microsystem that combines the biosensor microarray with chip-scale instrumentation electronics is of increasing interest. Due in part to advances in CMOS compatible fabrication of microelectrodes [24], [25], there is a trend to build sensor array microsystems that deposit sensor interfaces on the surface of silicon CMOS chips and interrogate the sensor elements with on-chip electronics [26]–[29].

Building on this trend, Fig. 1 illustrates the conceptual model of a CMOS electrochemical biosensor array microsystem that incorporates thermal control and readout electronics for an on-chip protein array. A silicon CMOS chip forms the substrate of the microsystem and incorporates circuitry for real time temperature control and measurement of biosensor activities including microhotplates, a programmable thermal controller, and an electrochemical readout circuit. Electrodes formed on the surface using post-CMOS fabrication techniques can be individually modified using molecular self assembly processes to form an array of protein interfaces [30]. Post-CMOS encapsulation with insulating materials protects the CMOS chip and enables operation within a liquid environment by combining with microfluidics or, as shown in Fig. 1, providing a fluid reservoir on the surface of the chip.

For both protein characterization and biosensing application modes, the ability to set the temperature of each array element independently is desirable. To achieve this goal, Fig. 1 illustrates that each array site contains an individual microhotplate with heater and sensor layers. The microhotplate array is connected to a multi-channel thermal control circuit that sets the temperature of each site to a programmed value. Because the microhotplate layers are very near the surface of the chip, the temperature of the protein interface can be well maintained. On-chip electrochemical readout circuitry connected to the surface electrode at each array site can then be used to characterize the protein interface responses over temperature or to interrogate a protein biosensor at its temperature of maximum reactivity. To maintain accuracy of the electronics within a chip that is constantly changing temperature, temperature-independent voltage, V_{ref}, and current, I_{ref} reference generators are included.

III. Microhotplate Array Design

A microhotplate is a micro-scale structure consisting of a resistive heater and a resistive temperature sensor that has been widely employed in microsystems. Most of the published microhotplates were designed for gas sensors, where the high temperatures required demand post-CMOS processing (bulk etching, etc.) to remove silicon beneath the hotplate and improve thermal isolation in air [31]–[33]. However, biosensors have a significantly lower temperature range, typically less than 60°C, which permits the opportunity to explore the design of a hotplate array without the complexity of post-CMOS thermal isolation process steps. In addition, biosensors are operated in liquid while gas sensors are operated in air, significantly changing the thermodynamic properties of the environment. To the best of our knowledge, the only microhotplate designed for biological applications and used within liquid environments with no post-CMOS process was constructed for cell culturing and incubation [34]. This device reported achieving a single fixed temperature of 37°C on the back side of a CMOS chip. In contrast, the reported protein array microsystem must be capable of setting individual array sites to different temperatures, it should provide thermal uniformity across the microhotplate to ensure no local hot spots that could destroy a protein interface, and it should permit temperatures as close to 60°C as possible while considering tradeoffs in process complexity and compatibility with standard CMOS power levels.

To better understand their thermal behavior, microhotplate design options were simulated using the *CoventorWare* finite element analysis tool with the Electromagnetics and Heat Transfer modules. Design optimizations were performed based on the following requirements: ability to achieve temperatures near 60°C, high thermal uniformity across the hotplate to prevent damage to biointerfaces, low power consumption, high thermal strength to increase robustness, and compatibility with a standard CMOS process. These simulations demonstrated that, when properly designed, a standard CMOS microhotplate, using two polysilicon layers for a heater resistor and a resistive temperature sensor, could achieve the target temperatures

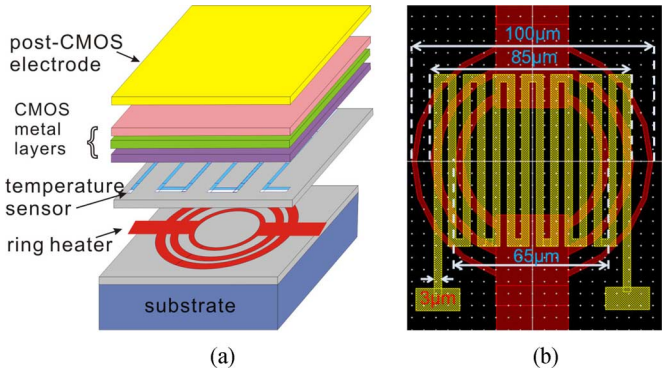

Fig. 2. (a) Cross section of the CMOS microhotplate for thermal control of on-chip biosensor arrays. (b) The heater and sensor layer geometries for an example microhotplate.

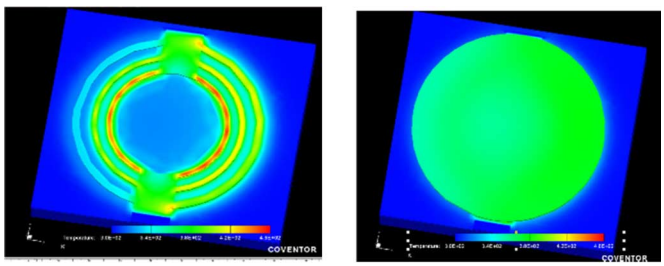

Fig. 3. Thermal analysis simulations. (a) Temperature probed at the heater surface. (b) Temperature probed on the top surface of the CMOS chip.

using only a 5 V supply and without any post-CMOS etching of silicon beneath the microhotplate for thermal isolation. Furthermore, simulations showed that sufficiently high temperatures could be achieved even in the presence of a liquid environment.

The simulated microhotplate array was then realized in the standard AMI 0.5 μm 3-metal, 2-poly CMOS process. The poly1 layer was used as the heater. A circular design was chosen to reduce heat dissipation [10]. To decrease resistance and thus increase power delivered, concentric rings were chosen rather than a single serpentine heater. The cross section of the CMOS microhotplate is presented in Fig. 2(a) and the microhotplate geometry is shown in Fig. 2(b). For a typical 100 μm diameter heater, the nominal heater resistance was set to 140 Ω, which was simulated to provide sufficient heating using only a 5 V supply. To analyze the thermal performance, the microhotplate has been simulated by CoventorWare. While the tetrahedrons mesh can cause the asymmetric results, the tetrahedrons mesh model was still chose in simulation due to its high accurate for complicated geometries, such as ring, round corner, sidewalls [35]. The thermal simulation of this structure in Fig. 3(a) shows hotter areas where current density is higher. Due to the small diameter of the heater and the desire to keep resistance low, limited control of hot spots can be achieved just by changing the poly1 layout. However, proper allocation of highly thermally conductive CMOS metal layers and via contacts between the heater and the surface electrode can minimize the lateral thermal gradient [10] and remove all local hot spots from the surface, as shown in Fig. 3(b). Moreover, the temperature uniformity of heaters with different surface areas can be achieved by properly adjusting layer shapes and geometries. The final element of the microhotplate is the resistive temperature sensor, which was formed in poly2 because of its higher sheet resistance and close proximity to the poly1 heater layer. The R-Squared linear regression of the temperature verse to the temperature sensor resistance is around 0.999 at 25–85°C, which presents the temperature sensor has good linearity. The temperature sensor resistor was laid out in a thin-wire serpentine pattern to average temperature across the heater area while producing a large resistance, nominally 300–400 kΩ, which helps to minimize errors due to the self-heating effect.

The top layer in each microhotplate is the surface electrode, which is fabricated after foundry CMOS to provide an anchor for immobilization of protein interfaces. Biointerfaces are typically implemented on chemically inert metals that will not degrade in a liquid environment. Gold is often chosen because of its binding properties with biointerfaces and its compatibility with post-CMOS fabrication using a titanium adhesion layer. Note that, for biointerfaces that demand electrodes with nanoscale smoothness, design of the CMOS metal layers beneath the surface electrode must be carefully considered to avoid unwanted steps in surface topology, which varies with the planarization methods of each CMOS process [30].

IV. Thermal Control and Readout Circuits

A. Thermal Controller

Precise thermal control is desirable to ensure a constant temperature throughout a measurement cycle. An on-chip thermal controller that manages feedback between the hotplate heater and temperature sensor can provide the desired temperature control. There are generally two types of thermal controller: proportional integral derivative (PID) and 'bang-bang' controller. The PID controller is more accurate and complicated than 'bang-bang' controller. Because the temperature resolution is loose for our application, 'bang-bang' controller meet the requirement. Because the microhotplates consume many of the CMOS layers, circuitry must be placed on the periphery of the array, as shown in Fig. 1. Thus, in designing the thermal controller, hardware efficiency is important in order to maximize the chip area available for the microhotplate array. An 'bang-bang' thermal controller was selected because it is more hardware efficient than a PID thermal controller [36]. The schematic in Fig. 4 describes the structure and operation of the implemented CMOS analog thermal controller whose main task is to ensure that the temperature on the microhotplate matches the desired temperature set point voltage, $\mathrm{T_{set}}$. The relation between the desired temperature and $\mathrm{T_{set}}$ was calibrated through independent measurement of sensor $\mathrm{R_S}$ resistance value over the temperature range of interest.

In the initial state of the analog thermal controller, the feedback voltage $(\mathrm{V_{fb}})$ is set as "0", which causes the output of the comparator to generate a "1" and thus turns on the NMOS switch SW that activates the resistive heater $\mathrm{R_H}$. As the microhotplate temperature increases, the resistance of the temperature sensor $\mathrm{R_S}$ decreases slightly due to its negative temperature coefficient of resistance (TCR). The temperature sensing

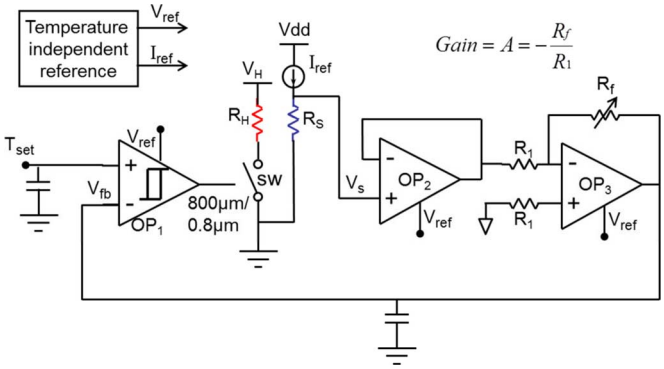

Fig. 4. Simplified schematic of the analog thermal controller.

voltage V_S feeds back to the negative input of the hysteresis comparator (OP_1) through a gain stage composed of OP_2 and OP_3. SW stays closed until V_{fb} becomes higher than T_{set}. The desired T_{set} is an input provided by an off-chip programmable voltage source. The hysteresis comparator was selected because it inherently improves system stability and reduces the thermal noise at V_{fb}. The switch frequency of SW is not high, generally less than 100 Hz because the temperature increase slope is less than tens-second/°C. In consider the electromagnetic field caused by SW switching, the SW is place far away the core circuit of thermal controller.

The typical TCR of the temperature sensor (R_S) is around $-1,000--3,500$ ppm/°C for the AMI 0.5 μm 3-metal, 2-poly CMOS process. Thus, the temperature coefficient (TC) of the temperature sensor voltage (V_S) can vary from 3 to 10.5 mV/°C for an around 150 kΩR_S (the resistance variation can be up to 20% in AMI 0.5 μm CMOS process) with 20 μA reference current (I_{ref}). However, 3 mV/°C is less than the hysteresis potential of OP_1, which was set to 15 mV. To ensure the TC at V_{fb} is larger than 15 mV, V_S is amplified through OP_3 by a gain of $A = -(R_f/R_1)$, where R_f is a programmable resistor array. The thermal feedback gain A was designed to be set as 1, 2, 4, or 8 according to the programmed value of R_f.

To reach desired temperatures, current on the order of 10 mA must pass through the resistive heater, R_H and the NMOS switch (SW). To ensure most of the voltage drops across R_H, SW has to be large to minimize resistance [23]. To achieve this goal, $W/L = 800\ \mu m/0.8\ \mu m$ was selected for SW.

B. Temperature Independent Reference Design

The accuracy of the temperature sensor voltage V_S is important for the resolution of the thermal controller. V_S should only be sensitive to the sensor resistance R_S, and thus the current flowing through R_S should be independent of temperature. Therefore, a temperature independent current source, I_{ref} is critical for the thermal control system. Accurate current and voltage references are also essential for properly biasing analog components in integrated circuits because the performance of nonlinear analog components depends strongly on the current flowing through them [37].

A temperature independent reference that is widely used because of its high accuracy utilizes two voltages having

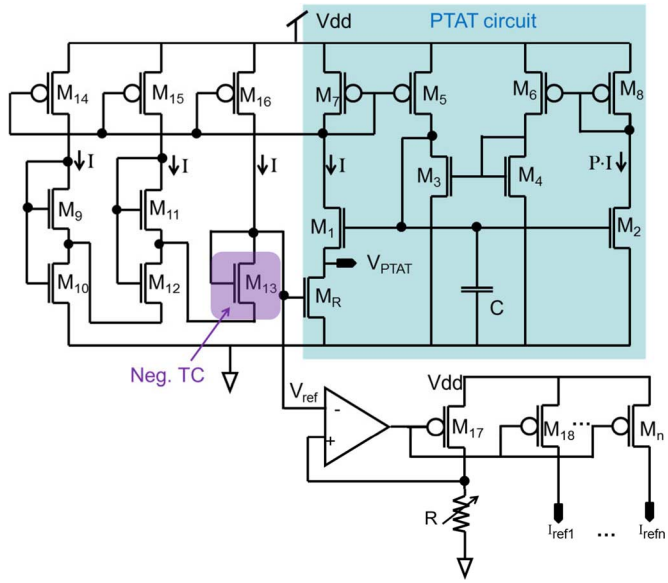

Fig. 5. Schematic of the temperature independent voltage and current reference generator.

opposite temperature coefficients that are added together to produce a voltage with a near-zero temperature coefficient [38]–[42]. In our design, the positive TC voltage was realized by circuits associated with a proportional to absolute temperature (PTAT) voltage that can also be used to monitor the ambient temperature. The negative temperature coefficient was achieved through the threshold voltage of an NMOS transistor. The schematic of the temperature independent reference circuit is shown in Fig. 5. In the PTAT circuit, we have replaced the traditional resistor with nMOS transistor M_R that operates in the deep triode region. This reduces circuit area and increases accuracy by avoiding the temperature coefficient of a passive resistor. $M_1 - M_2$ and $M_9 - M_{13}$ are designed to operate in the sub-threshold region to minimize the power consumption. The output reference voltage V_{ref} can be expressed as

$$V_{ref} = V_{GS13} + (V_{GS11} - V_{GS12}) + (V_{GS9} - V_{GS10}). \quad (1)$$

Because $M_9 - M_{13}$ operate in the sub-threshold region, (1) can be rewritten as

$$V_{ref} = V_{GS13} + \eta V_T \left(\frac{2(W/L)_{10}(W/L)_{12}}{(W/L)_9(W/L)_{11}} \right) \quad (2)$$

$$V_{ref} = V_{TH} + \eta V_T \ln \left[\frac{3I}{(W/L)_{13} I_0} \right] + \eta V_T \ln \left[\frac{2(W/L)_{10}(W/L)_{12}}{(W/L)_9(W/L)_{11}} \right] \quad (3)$$

where W/L is the transistor size ratio, V_{GS} is the gate-source voltage, V_{TH} is the threshold voltage, $I_0 = \mu C_{0x}(\eta - 1)V_T$, η is the sub-threshold slope factor, $V_T (= k_B T/q)$ is the thermal voltage (where k_B is Boltzmann constant, T is the absolute

temperature, q is the elementary charge), and I is the current through $\mathrm{M_R}$ given by

$$\mathrm{I} = \mathrm{I_{DSR}} = \frac{\mathrm{V_{DSR}}}{\mathrm{R_R}} = \left(\frac{\mathrm{W}}{\mathrm{L}}\right)_{\mathrm{R}} \mu_{\mathrm{n}}\mathrm{C_{ox}}(\mathrm{V_{ref}} - \mathrm{V_{TH}})\eta\mathrm{V_T} \ln\left(\frac{\mathrm{P(W/L)_1}}{\mathrm{(W/L)_2}}\right). \quad (4)$$

Combining (3) and (4), (3) can be rewritten as

$$\mathrm{V_{ref}} = \mathrm{V_{TH}} + \eta\mathrm{V_T} \ln\left[\frac{3\mu_{\mathrm{n}}\mathrm{C_{ox}(W/L)_R}}{\mathrm{(W/L)_{13}I_0}} \ln\left(\frac{\mathrm{P\,(W/L)_1}}{\mathrm{(W/L)_2}}\right)\right] + \eta\mathrm{V_T} \ln\left[\frac{2\mathrm{(W/L)_{10}(W/L)_{12}}}{\mathrm{(W/L)_9(W/L)_{11}}}\right] \quad (5)$$

where $V_{TH} = V_{TH0} - \kappa T$, V_{TH0} is the threshold voltage at 0 K and κ is a constant value. From (5), we find that the output of the reference $(\mathrm{V_{ref}})$ equals to the transistor threshold voltage at 0 K. As a result, the minimum supply voltage could be as low as $\mathrm{V_{TH0}} + 0.2$ V (assuming a minimum FET drain-source voltage of 0.2 V).

The temperature coefficient of $\mathrm{V_{ref}}$ can be expressed as

$$\frac{\partial \mathrm{V_{ref}}}{\partial \mathrm{T}} = -\kappa + \frac{\eta\kappa_{\mathrm{B}}}{\mathrm{q}} \times \ln\left[\frac{6\eta\mathrm{q\,(W/L)_{10}\,(W/L)_{12}\,(W/L)_R}}{\kappa_{\mathrm{B}}\,(\eta-1)\,\mathrm{(W/L)_9\,(W/L)_{11}\,(W/L)_{13}}} \times \ln\frac{\mathrm{p\,(W/L)_1}}{\mathrm{(W/L)_2}}\right]. \quad (6)$$

In (6), the first term is negative and the second term is positive, which shows that a temperature independent voltage reference $(\partial V_{ref}/\partial T = 0)$ can be generated by properly setting the size of transistors $\mathrm{M_1}$, $\mathrm{M_2}$, $\mathrm{M_R}$, and $\mathrm{M_9} - \mathrm{M_{13}}$.

Once the temperature independent voltage $\mathrm{V_{ref}}$ was created, a series of temperature independent current reference $\mathrm{I_{ref1}} \ldots \mathrm{I_{refn}}$ could readily be generated. As shown in Fig. 5 this was achieved by implementing a voltage to current convertor and current mirrors. The off-chip trimmer resistance R allows the value of $\mathrm{I_{ref}}$ to be adjusted during testing.

C. Electrochemical Readout Circuit

Electrochemical impedance spectroscopy (EIS) is a powerful method for the characterization of biointerface reactions [43]. For example, EIS allows fast monitoring of important biomolecular interaction parameters such as binding constants, affinity rate, and surface reactivity. The EIS technique is generally accomplished by sweeping the frequency of a small (1–10 mV) sinusoidal voltage stimulus and measuring the resulting AC current. Using micro-electrodes, the current of biointerface reactions can be down into the sub-pA level. Thus, in order to address the measurement challenges set by sub-pA currents, a low-noise readout circuit is essential.

To support chip-scale microsystem applications, a high-sensitivity compact impedance-to-digital converter (CIDC) circuit was developed for the thermal control chip based on our previous work [44], [45]. The CIDC circuit can monitor the activities of protein interfaces by extracting the amplitude/phase or real/imaginary portions of the impedance response. Each CIDC channel includes low noise current readout, analog-domain impedance component extraction and local digitization.

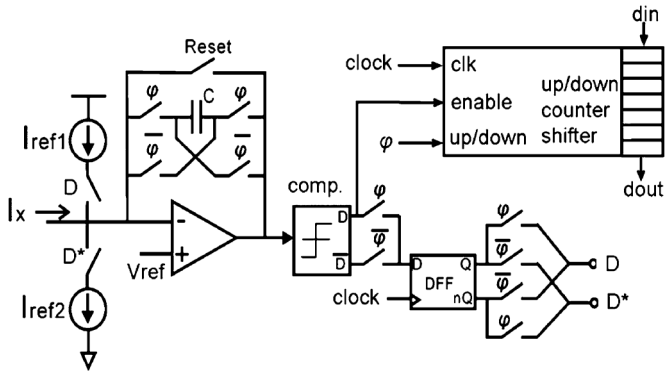

Fig. 6. Simplified compact impedance-to-digital converter structure. φ is the reference square wave.

To measure sub-pA AC current signals, the CIDC circuit combines lock-in and oversampling techniques. The lock-in technique, also known as a phase-sensitive detection, is widely used to detect and measure very small AC signals from an extremely noisy environment. Using the oversampling technique, the built-in sigma-delta ADC achieves good antialiasing and high resolution in the low to mid frequency range appropriate for protein interface characterization.

The CIDC is based on a sigma-delta ADC structure, as shown in Fig. 6. It includes a lock-integrator stage to realize impedance component extraction and a flip-flop and a bidirectional counter for digitization. Without the switches controlled by φ, the structure is similar to a traditional sigma-delta ADC, where the comparator is a 1-bit ADC and the reference currents form a 1-bit DAC. Further details of the design concept and mathematical analysis are presented in [44].

V. Package

A 3×3 microhotplate array chip was fabricated in 0.5 μm CMOS and was wire bonded to a standard DIP40 package for electrical testing. To conduct thermal tests in a liquid environment, a simple packaging scheme that circumvents photolithography was developed to enable liquid to get to the chip surface without interfering with wire bond connections. The area around the chip, inside the DIP40 package, was filled with SU8 photoresist. SU8 is commonly used to construct microstructures because it can form thick layers and is available in a wide range of viscosities. Also SU8 provides thermal insulation for the chip resulting in reduced heat loss to the ambient air. Because the volume of the chip package is much greater than the size of the chip, there is a large volume to fill. The SU8 was applied through a syringe in several layers, and soft baking on a hotplate and cross linking with UV light was then performed on each layer sequentially, as shown in Fig. 7. While applying SU8 solution, surface tension holds the material to the objects it is in contact with and tends to prevent spreading, depending on its viscosity. Lower viscosity SU8 was found to fill the package

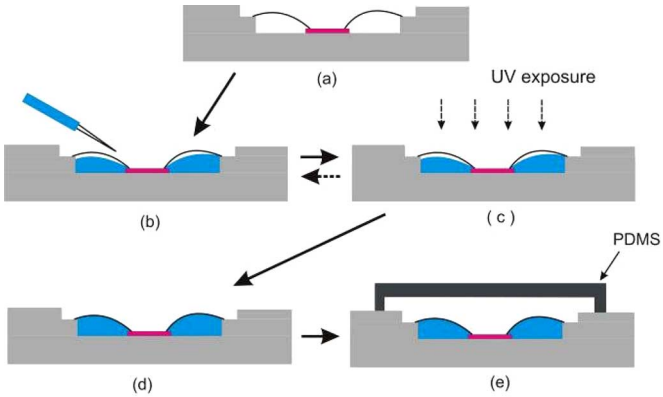

Fig. 7. Chip packaging process flow. (a) Chip in DIP40. (b) Dispense SU8 2002 using a syringe. (c) Soft baking, UV exposure and hard baking. (d) Final SU8 reservoir. (e) PDMS cap on DIP40 package. Steps (b) and (c) are repeated 4 or 5 times until package is fully filled with SU8.

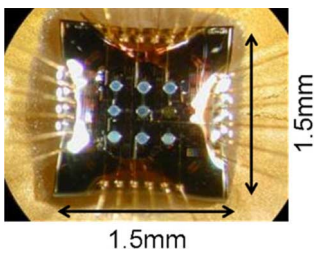

Fig. 8. 1.5 mm × 1.5 mm wire bonded microhotplate array chip encapsulated with SU8 2002. The chip contains a 3 × 3 microhotplate array.

quickly and uniformly, but it would flood over the chip surface easily. When applied to bonding wires, SU8 of higher viscosity would not spread onto the center of the chip, but it could not coat the wires very well. Experiments were performed to determine which viscosity of SU8 provided the ideal combination of uniform coverage of the large package volume with sufficient surface tension to deter spreading onto the surface of the chip. SU8 2002 was found to be most effective.

The final SU8 layer insulated the wire bonds and created a reservoir of approximately 0.5 ml above the chip, as shown in Fig. 8. To extend the reservoir volume, a polymethylsiloxane (PDMS) cap was fabricated using an SU8 master and soft lithography techniques that are standard for this biocompatible material. The cap extended the height of the reservoir by about 400 μm, increasing the volume to approximately 1 ml. The PDMS structure was found to seal well to the SU8 chip packaging and hold liquid samples during thermal testing.

VI. Test Results

To develop the thermal control protein array microsystem, two different test chips were designed and characterized. The first was a passive microhotplate array chip (without CMOS circuits) that enabled extensive microhotplate characterization and determination of thermal control circuit parameters. The second chip utilized the tested microhotplate design and added on-chip thermal control and electrochemical readout circuits.

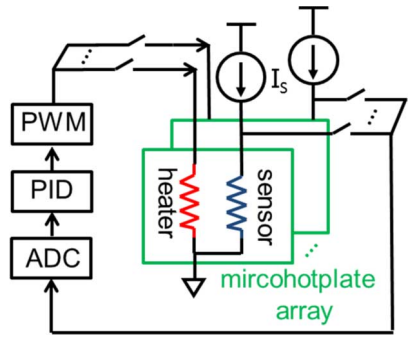

Fig. 9. The structure of the test board for the microhotplate array chip.

A. Microhotplate Array Test Results

To calibrate the performance of the microhotplate array in a liquid environment, a test board was developed to connect the microhotplate array chip to a PC equipped with a data acquisition card (DAQ). The structure of the test board is shown in Fig. 9. In this multi-channel test board, a temperature-independent current, Is, generates a proportional-to-temperature voltage that is read by an A/D converter. A PID thermal controller implemented in software compares the expected temperature with the sensor-measured temperature and adjusts the duty cycle of the pulse width modulator (PWM). The PWM controls the heater to deliver the average power necessary to maintain the desired temperature.

The chip was first placed in a temperature control chamber (Bma-bryant, AH-202XS) to determine the poly1 sensor resistor's TCR. The poly1 resistance was found to decrease linearly with temperature from 27–80°C, and a TCR of $-1{,}520$ ppm/°C was calculated, with similar results for all sensor resistors on the chip. To improve measurement precision, the TCR for each chip must be calibrated individually because TCR is process sensitive.

After calibrating the external PID controller, a step response test of the entire thermal control system was performed at room temperature by setting the desired temperature from 27 to 42°C in 3°C steps. The temperature was held constant for 60 seconds at each step. The results plotted in Fig. 10 show that the thermal settling time increases with temperature, as expected, with the 3°C step to 30°C taking about 14 seconds. Once the set point is reached, the temperature is held very stable by the feedback controller; extensive testing shows a maximum error of only 0.7°C over the entire span of operation. When the microhotplate is held at a set temperature for a long time (over ten minutes), the temperature of the microhotplate was observed to shift slightly. This phenomenon was observed to be stronger with higher set temperatures.

The heating potential of the on-chip microhotplate as a function of heater voltage was tested in both air and liquid environments. The results in Fig. 11 show that, as expected, higher voltages generate higher maximum temperatures. Although the maximum temperature is slightly higher in air, the microhotplate in liquid was able to rise to nearly 45°C with only a 5 V heater drive voltage. Because the heater drive voltage connects only to the heater resistor and not to CMOS circuitry, a higher voltage could be used to increase the temperature. However,

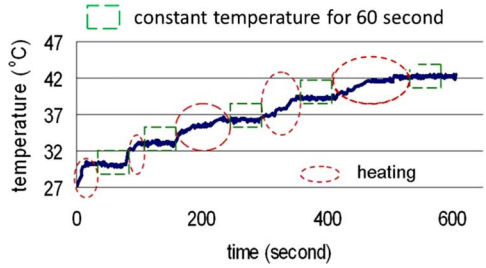

Fig. 10. Thermal step response of the microhotplate thermal control system for 3°C steps.

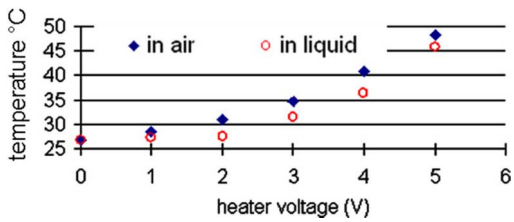

Fig. 11. Temperature (at on-chip sensor) in air and in liquid at different heater voltages.

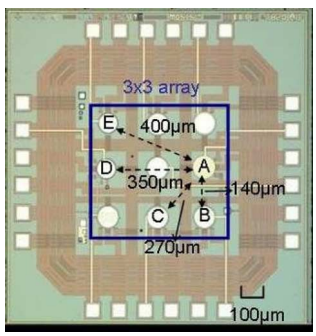

Fig. 12. Die photograph of the 1.5 mm × 1.5 mm microhotplate 3 × 3 array. The diameter of each microhotplate is 100 μm.

45°C is sufficient to characterize most proteins or to maximize their reactivity for sensor applications. For example, our colleagues [11] have characterized the temperature dependence of NEST (NEST is a hydrophobic recombinant polypeptide comprising the catalytic domain (residues 727–1216) of neuropathy target esterase [46]), a catalytically active fragment of the membrane protein Neuropathy Target Esterase (NTE) found in human neurons. The NEST thermal characteristics in the range of 20°C—60°C, show a typical parabolic function with maximum activity at 31°C after which activity irreversibly degrades. The microhotplate array microsystem is well suited to thermally control this and similar proteins.

Finite element analysis simulations predicted that the heat from each array element would be contained in very close proximity to the heating element, even without additional processing steps to improve the thermal isolation of each heater. To test this prediction, an experiment was conducted where one array element was heated and the temperature sensors of several other array elements were monitored. Referring to labels in Fig. 12, a 5 V source was applied to the heater in array element 'A' for more than 10 min to ensure the maximum temperature was reached. Microhotplate temperature sensor values at elements

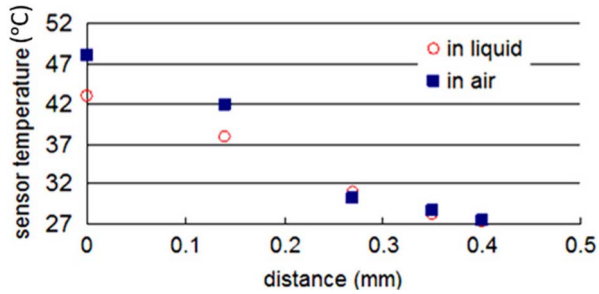

Fig. 13. The sensor measured temperature versus the distance from the heating source to the sensor.

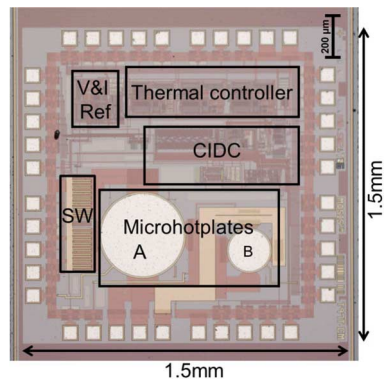

Fig. 14. Die photograph of the thermal control and detection chip. The diameter of the microhotplate A and B is 400 μm and 200 μm, respectively.

'A'—'E' were then recorded. Fig. 13 plots the results as a function of the sensor's distance from the one active heater, 'A'. As expected, as distance increases the thermal isolation improves, and at only 0.4 mm from the heater the induced temperature change is less than 1°C. Although the thermal isolation was not as strong as predicted by simulations, these results verify that heating is sufficiently self-contained heating to permit each array element to be set to a different temperature for simultaneous characterization at multiple temperatures.

B. Thermal Control Chip Test Results

After characterizing the thermal performance of the microhotplate array chip, the thermal control and detection chip shown in Fig. 14 was designed and fabricated in the same 0.5 μm CMOS process. Two CMOS thermal control channels, two CIDC readout channels, and two microhotplates with 100 μm and 200 μm diameter were integrated in the 1.5 mm × 1.5 mm chip.

To test the CIDC EIS readout circuit, a DAQ card (Agilent, USB6259) was used to generate the sinusoid stimulus voltage, reference square wave, global clock and digital control signals, and to record digital outputs from the CIDC circuit. An equivalent RC impedance circuit for a biomimetic membrane sensor interface [3] was utilized to characterize the performance of the CIDC circuit. Fig. 15 illustrates this test setup. To verify CIDC impedance component extraction capability, the biosensor model was stimulated with a sinusoidal voltage over a 0.1 to 100 Hz frequency range. Fig. 16 plots the *real* and *imaginary* results obtained from the digital output of the CIDC. The theoretical curve for the model impedance also

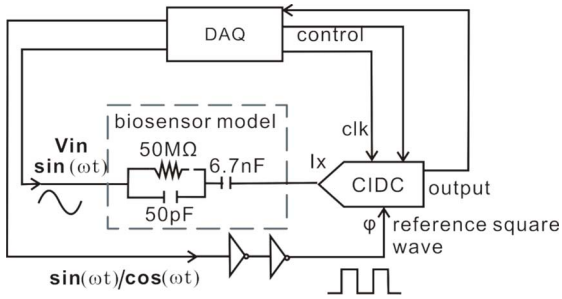

Fig. 15. Test platform for the CIDC circuit with a biosensor equivalent circuit model.

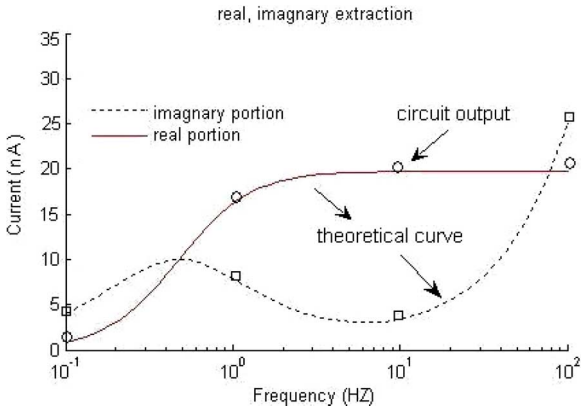

Fig. 16. The real and imagineary portions of EIS current response along with theoretical (expected) curve for comparision.

plotted in Fig. 16 shows that the CIDC tracks both components of impedance very well, with a maximum mismatch of 1% of the full scale response. The power consumption of one CIDC channel was measured as 5.2 μW with 3.3 V power supply and a 200 kHz clocking frequency. This low power consumption enables long battery-life for portable applications and protects on-chip biosensors from undesirable self heating. The CIDC occupies 0.045 mm^2 per channel, permitting 200 channels within a 3 mm $\times$ 3 mm die area.

To measure the accuracy of the temperature independent reference voltage and current generator, the thermal control and detection chip was placed in a programmable temperature control chamber (Bma-bryant, AH-202XS) that is controlled by a PC through an RS232/GPIB interface. The output reference voltage and current signals from the biasing circuit were record by the DAQ card. The measured reference voltage and current from 10 to 70°C are plotted in Fig. 17 and show a temperature variation of less than 347 ppm/°C and 167 ppm/°C, respectively. Thus, the variation at V_s caused by the current reference is around 0.7 mV/°C, which is significantly less than the V_S variation generated by temperature sensor resister, R_S.

To measure the analog thermal controller performance, a linearity response test of the entire thermal control circuit was performed in air at room temperature (25°C) by setting the desired electrode temperature from 25 to 50°C in 3°C step. There is overshoot in the bang-bang control, so the temperature window of the hysteresis comparator was set as ± 0.5°C. Also, the switch noise and the offset of the hysteresis comparator impact the resolution. The results plotted in Fig. 18 show that the temperature was held stable by the feedback controller with a maximum error of ± 1° C over the entire duration of operation once the set point was reached. The response time was less than one minute for all 3°C steps.

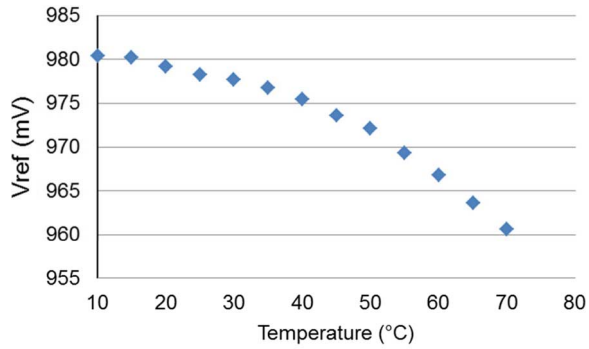

(a)

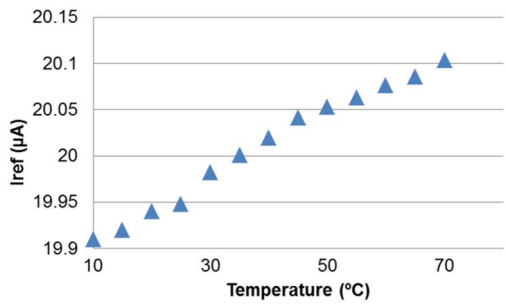

(b)

Fig. 17. Measured outputs of (a) voltage (b) and current references versus temperature from 10°C to 70°C.

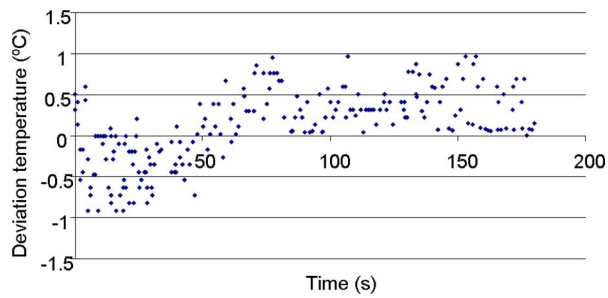

Fig. 18. The deviation between set point temperature (Temp_set) and measured temperature for 25°C to 50°C with gain = 2 setting measured 180 second.

VII. Conclusion

A CMOS microhotplate was presented that ensures good spatial uniformity with no local hotspots and provides the temperature range and array isolation suitable for protein-based biosensors. A microhotplate array chip was fabricated in a standard CMOS process and packaged using layering of SU8 for use in a liquid environment. A maximum temperature of 45°C was achieved in liquid with a 5 V supply, and array elements were tested to be almost completely thermally isolated from each other at distances beyond 0.4 mm without any post-CMOS processing. Based on these results, a CMOS thermal control and impedance detection chip-scale microsystem for protein biosensor applications was developed and tested. This chip was

shown to provide accurate readout and extraction of impedance components with a low power, compact circuit suitable for array implementation. The thermal control circuitry was shown to set and hold temperatures within $\pm 1^{\circ}$ C. The results of this work enable the realization of a high density CMOS thermal control microsystem array for characterization of protein biointerfaces or highly sensitive protein-based biosensors.

ACKNOWLEDGMENT

Support from the MOSIS Service and the assistance of Y. Huang with thermal simulations is gratefully acknowledged.

REFERENCES

[1] J. Drews, "Drug discovery: A historical perspective," *Science*, vol. 287, pp. 1960–1964, 2000.
[2] D. J. Cahill, "Protein arrays: A high-throughput solution for proteomics research?," *Proteomics: A Trends Guide (Trends Biotechnol.)*, pp. 47–51, 2000.
[3] S. J. Maerkl, "Next generation microfluidic platforms for high-throughput protein biochemistry," *Current Opin. Biotechnol.*, vol. 22, pp. 1–7, 2010.
[4] A. Bard and L. Faulkner, *Electrochemical Methods: Fundementals and Applications*, 2nd ed. New York, NY, USA: Wiley, 2000.
[5] P. Auroux, D. Iossifidis, D. R. Reyes, and A. Manz, "Micro total analysis systems 2. Analytical standard operations and applications," *Anal. Chem.*, vol. 74, pp. 2637–2652, 2002.
[6] V. N. B. Samel, A. Russom, P. Griss, and G. Stemne, "A disposable lab-on-a-chip platform with embedded fluid actuators for active nanoliter liquid handling," *Biomed Microdev.*, vol. 9, pp. 61–67, 2007.
[7] B. Hassler, N. Kohli, J. Zeikus, I. Lee, and R. Worden, "Renewable dehydrogenase-based interfaces for bioelectronic applications," *Langmuir*, vol. 23, pp. 7127–7133, 2007.
[8] M. G. U. Frey, S. Taschini, K. U. Kirstein, and A. Hierlemann, "A digital CMOS architecture for a micro-hotplate array," *IEEE J. Solid-State Circuits*, vol. 42, pp. 441–450, 2007.
[9] S. Semancik *et al.*, "Microhotplate platforms for chemical sensor research," *Sens. Actuators B, Chem,*, vol. B77, pp. 579–591, 2001.
[10] A. Hierlemann, *Integrated Chemical Microsensor Systems in CMOS Technology*. New York, NY, USA: Springer, 2005.
[11] X. Liu, L. Li, and A. J. Mason, "Thermal control microsystem for protein characterization and sensing," in *Proc. IEEE Biomedical Circuits Systems Conf.*, Nov. 2009, pp. 277–280.
[12] J. V. Cannon and D. P. Lane, "Protein synthesis required to anchor a mutant p53 protein which is temperature-sensitive for nuclear transport," *Lett. Nature*, vol. 349, pp. 802–806, 1991.
[13] M. Nakamura *et al.*, "Optimal temperature for synthesis of DNA, RNA, and protein by human testis in vitro," *Arch Androl.*, vol. 20, pp. 41–44, 1988.
[14] P. Novick and D. Botstein, "Phenotypic analysis of temperature-sensitive yeast actin mutants," *Cell*, vol. 40, pp. 405–416, 1985.
[15] S.-L. Chang and N. Tjandra, "Temperature dependence of protein backbone motion from carbonyl ^{13}C and amide ^{15}N NMR relaxation," *J. Magn. Reson.*, vol. 174, pp. 43–53, 2005.
[16] S.-L. Chang, A. Szabo, and N. Tjandra, "Temperature dependence of domain motions of calmodulin probed by NMR relaxation at multiple fields," *J. Amer. Chem. Soc.*, vol. 125, pp. 11379–11384, 2003.
[17] L. Spyracopoulos *et al.*, "Temperature dependence of dynamics and thermodynamics of the regulatory domain of human cardiac troponin C," *Biochem.*, vol. 40, pp. 12541–12551, 2001.
[18] H. Zhu and M. Snyde, "Protein arrays and microarrays," *Current Opin. Chem. Biol.*, vol. 5, pp. 40–45, 2001.
[19] W. Rychlik, W. J. Spencer, and R. E. Rhoads, "Optimization of the annealing temperature for DNA amplification in vitro," *Nucl. Acids Res.*, vol. 18, pp. 6409–6412, 1990.
[20] C. Schildkraut and S. Lifson, "Dependence of the melting temperature of DNA on salt concentration," *Biopolymers*, vol. 3, pp. 195–208, 1965.
[21] G. P. Brewood *et al.*, "Electrical detection of the temperature induced melting transition of a DNA hairpin covalently attached to gold interdigitated microelectrodes," *Nucl. Acids Res.*, vol. 36, p. E98, 2008.
[22] C. Yi, C. Li, S. Ji, and M. Yang, "Microfluidics technology for manipulation and analysis of biological cells," *Analytica Chimica Acta*, vol. 560, pp. 1–23, 2006.
[23] R. Sathuluri, S. Yamamura, and E. Tamiya, "Microsystems technology and biosensing," *Adv. Biochem. Eng./Biotechnol.*, vol. 109, pp. 285–350, 2008.
[24] M. Schienle *et al.*, "A fully electronic DNA sensor with 128 positions and in-pixel A/D conversion," *IEEE J. Solid State Circuits*, vol. 39, pp. 2438–2445, Dec. 2004.
[25] F. Heer *et al.*, "CMOS microelectrode array for bidirectional interaction with neuronal networks," *IEEE J. Solid State Circuits*, vol. 41, pp. 1620–1629, 2006.
[26] B. Eversmann *et al.*, "A 128 × 128 CMOS biosensor array for extracellular recording of neural activity," *IEEE J. Solid State Circuits*, vol. 38, pp. 2306–2317, 2003.
[27] L. Li, X. Liu, and A. Mason, "CMOS amperometric instrumentation and packaging for biosensor array applications," *IEEE Trans. Biomed. Circuits Syst.*, vol. 5, pp. 439–448, 2011.
[28] X. Zhu and C. Ahn, "On-chip electrochemical analysis system using nanoelectrodes and bioelectronic CMOS chip," *IEEE J. Sensors*, vol. 6, pp. 1280–1286, Oct. 2006.
[29] H. Mazhab-Jafari, L. Soleymani, and R. Genov, "16-channel CMOS impedance spectroscopy DNA analyzer with dual-slope multiplying ADCs," *IEEE Trans. Biomed. Circuits Syst.*, vol. 6, pp. 468–478, 2012.
[30] Y. Huang, Y. Liu, B. Hassler, R. M. Worden, and A. J. Mason, "A protein-based electrochemical biosensor array platform for integrated microsystems," *IEEE Trans. Biomed. Circuits Syst.*, vol. 7, no. 1, pp. 43–51, Feb. 2013.
[31] R. Casanova, J. Merino, L. Dieguez, S. Bota, and J. Samitier, "A mixed-mode temperature control circuit for gas sensors," in *Proc. IEEE Int. Symp. Circuits and Systems*, 2004, pp. 896–899.
[32] U. Frey, M. Graf, S. Taschini, K. U. Kirstein, and A. Hierlemann, "A digital CMOS architecture for a micro-hotplate array," *IEEE J. Solid State Circuits*, vol. 42, pp. 441–450, 2007.
[33] R. E. C. S. Semancik, M. C. Wheeler, J. E. Tiffany, G. E. Poirier, R. M. Walton, J. S. Suehle, B. Panchapakesan, and D. L. DeVoe, "Microhotplate platforms for chemical sensor research," *Sens. Actuators B*, vol. 77, pp. 579–591, 2001.
[34] J. Christen and A. Andreou, "Design, fabrication, and testing of a hybrid CMOS/PDMS microsystem for cell culture and incubation," *IEEE Trans. Biomed. Circuits Syst.*, vol. 1, pp. 3–18, 2007.
[35] B. Pepin, CoventorWare Tutorial [Online]. Available: http://www-inst.eecs.berkeley.edu/~ee245/fa12/homework/CoventorWare_Tutorial.pdf 2011
[36] D. Barrettino *et al.*, "Hotplate-based monolithic CMOS microsystems for gas detection and material characterization for operating temperatures up to 500 C," *IEEE J. Solid State Circuits*, vol. 39, pp. 1202–1207, 2004.
[37] E. M. Camacho-Galeano, C. Galup-Montoro, and M. C. Schneider, "A 2-nW 1.1-V self-biased current reference in CMOS technology," *IEEE Trans. Circuits Syst. II, Exp. Briefs*, vol. 52, pp. 61–65, 2005.
[38] H. Banba *et al.*, "A CMOS bandgap reference circuit with sub-1-V operation," *IEEE J. Solid State Circuits*, vol. 34, pp. 670–674, 1999.
[39] K. N. Leung and P. K. T. Mok, "A sub-1-V 15-ppm/$^{\circ}$ C CMOS bandgap voltage reference without requiring low threshold voltage device," *IEEE J. Solid State Circuits*, vol. 37, pp. 526–530, 2002.
[40] F. Serra-Graells and J. L. Huertas, "Sub-1-V CMOS proportional-to-absolute temperature references," *IEEE J. Solid State Circuits*, vol. 38, pp. 84–88, 2003.
[41] K. Ueno, T. Hirose, T. Asai, and Y. Amemiya, "A 300 nW, 15 ppm/C, 20 ppm/V CMOS voltage reference circuit consisting of subthreshold MOSFETs," *IEEE J. Solid State Circuits*, vol. 44, pp. 2047–2054, 2009.
[42] D. F. Hilbiber, "A new semiconductor voltage standard," *IEEE J. Solid State Circuits*, vol. 2, pp. 32–33, 1964.
[43] O. A. Sadik *et al.*, "Differential impedance spectroscopy for monitoring protein immobilization and antibody-antigen reactions," *Anal. Chem.*, vol. 74, pp. 3142–3150, 2002.
[44] X. Liu, D. Rairigh, C. Yang, and A. J. Mason, "Impedance-to-digital converter for sensor array microsystems," in *Proc. IEEE Int. Symp. Circuits and Systems*, May 2009, pp. 353–356.
[45] X. Liu, D. Rairigh, and A. Mason, "A fully integrated multi-channel impedance extraction circuit for biosensor arrays," in *Proc. IEEE Int. Symp. Circuits and Systems*, 2010, pp. 3140–3143.
[46] M. Tienhoven, J. Atkins, Y. Li, and P. Glynn¶, "Human neuropathy target esterase catalyzes hydrolysis of membrane lipids," *J. Biol. Chem.*, vol. 277, pp. 20942–20948, 2002.

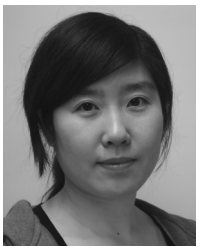

Xiaowen Liu (S'10) received the B.S. and M.S. degrees in electrical engineering from Hefei University of Technology, Heifei, China, in 2002 and 2005, respectively.

Currently, she is working toward the Ph.D. degree in electrical engineering at Michigan State University, East Lansing, MI, USA. From 2005 to 2007, she was an Analog Design Engineer in the Beijing Microelectronic Technology Institute, Beijing, China, where she was involved in the design of high frequency PLL frequency synthesizers. Her research interests include analog and mixed-signal integrated circuit design, biomedical electronics, and biomedical integrated microsystems.

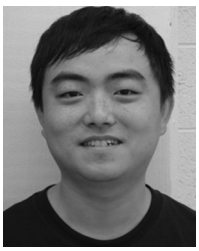

Lin Li received the B.S. degree in electrical engineering from Tsinghua University, Beijing, China, and the M.S. degree in electrical engineering from Michigan State University (MSU), East Lansing, MI, USA, in 2006 and 2012, respectively.

Currently, he is working toward the Ph.D. degree in electrical engineering at MSU. His research interests include on-CMOS electrochemical biosensor arrays, post-CMOS process and packaging, 3D microsystem integration, and membrane protein study.

Andrew J. Mason (S'90–M'99–SM'06) received the B.S. degree in physics with highest distinction from Western Kentucky University, Bowling Green, in 1991, the B.S.E.E. degree with honors from the Georgia Institute of Technology, Atlanta, GA, USA, in 1992, and the M.S. and Ph.D. degrees in electrical engineering from the University of Michigan, Ann Arbor, MI, USA, in 1994 and 2000, respectively.

From 1999 to 2001, he was an Assistant Professor at the University of Kentucky, Lexington, KY, USA. In 2001, he joined the Department of Electrical and Computer Engineering at Michigan State University, East Lansing, MI, USA, where he is currently an Associate Professor. His research explores mixed-signal circuits and microfabricated structures for integrated microsystems in biomedical and environmental monitoring applications. Current projects include wearable/implantable electrochemical and bioelectronic sensors systems, microfabricated electrochemical sensor arrays, array signal processing algorithms and hardware, and post-CMOS integration of sensing, instrumentation, and microfluidics.

Dr. Mason is a Senior Member of the Institute of Electrical and Electronic Engineers (IEEE) and serves on the Sensory Systems and Biomedical Circuits and Systems Technical Committees of the IEEE Circuits and Systems Society. He is an Associate Editor for IEEE TRANSACTIONS ON BIOMEDICAL CIRCUITS AND SYSTEMS and on the editorial board for the *BioNanoScience* journal. He regularly serves on the technical and review committees for several IEEE conferences and was co-General Chair of the 2011 IEEE Biomedical Circuits and Systems Conference. He was a recipient of the 2006 Michigan State University Teacher-Scholar Award and the 2010 Withrow Award for Teaching Excellence.